NATO UNCLASSIFIED

SACLANT UNDERSEA RESEARCH CENTRE REPORT

Bottom reflection properties deduced from ambient noise: simulation of a processing technique
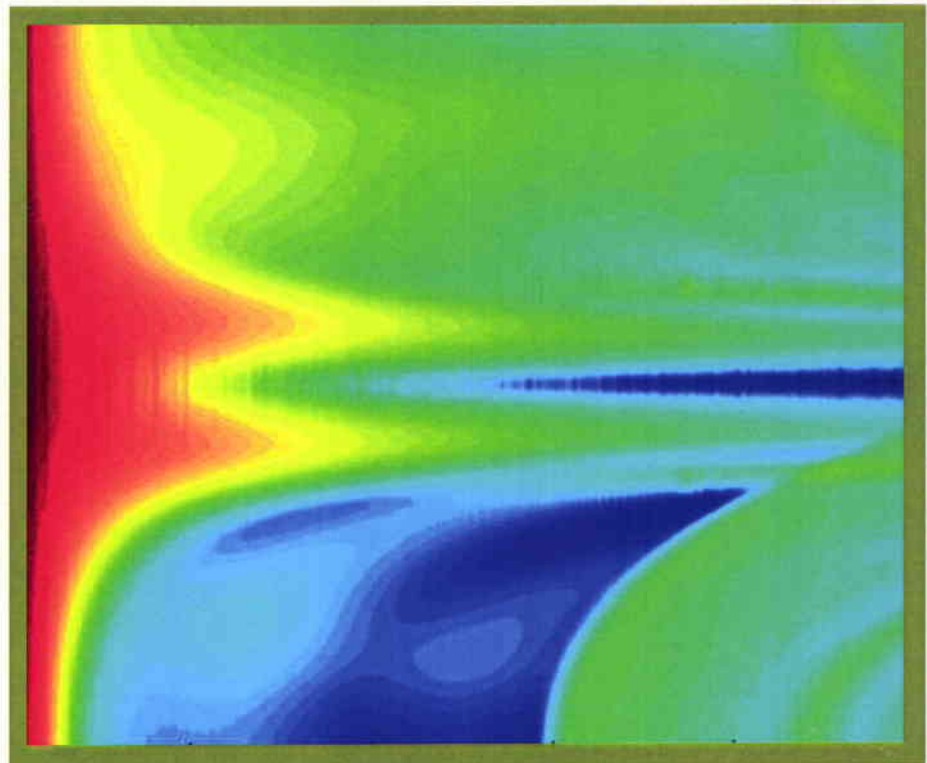
Chris H. Harrison, Alberto Baldacci

November 2002

NORTH ATLANTIC TREATY ORGANIZATION   ORGANISATION DU TRAITE DE L'ATLANTIQUE NORD

NATO UNCLASSIFIED

SACLANTCEN SM-392

Bottom reflection properties deduced from ambient noise: simulation of a processing technique

C H Harrison and A Baldacci

The content of this document pertains to work performed under Project 04C-3 of the SACLANTCEN Programme of Work. The document has been approved for release by The Director, SACLANTCEN.

Jan L. Spoelstra
Director

– ii –

intentionally blank page

Bottom reflection properties deduced from ambient noise: simulation of a processing technique

C H Harrison and A Baldacci

Executive Summary: Multipath propagation in shallow water is inevitably highly sensitive to seabed properties and therefore their geographic variation. This means that predictions of sonar performance and area coverage may be misleading if based on extrapolations rather than detailed surveys of bottom properties. A promising new method has already been proposed **[SACLANTCEN SM 387]** to calculate bottom reflection loss from ambient noise directionality. Surveying is well within its scope. Although this method has been tried experimentally at more than 11 sites under various conditions, it is difficult to explore its limitations exhaustively by experiment. In these cases numerical testing is much more straightforward. For example, array tilt, array curvature, and varying sound speed along the array are relatively easy to model. Numerical techniques are useful in eliminating contending effects and homing in on the correct one. They also provide a second opinion on the theoretical background of the experimental technique, and throw light on, for instance, the feasibility of using a drifting array as a bottom surveying tool. This report attempts to quantify problems such as these.

intentionally blank page

SACLANTCEN SM-392

Bottom reflection properties deduced from ambient noise: simulation of a processing technique

C H Harrison and A Baldacci

Abstract: A promising new method has already been proposed **[SACLANTCEN SM-387]** to calculate bottom reflection loss from ambient noise directionality. Although this method has been tried experimentally at more than 11 sites under various conditions, it is difficult to explore its limitations exhaustively by experiment. In these cases numerical testing is much more straightforward. For example, array tilt, array curvature, and varying sound speed along the array are relatively easy to model. Numerical techniques are useful in eliminating contending effects and homing in on the correct one. They also provide a second opinion on the theoretical background of the experimental technique, and throw light on, for instance, the feasibility of using a drifting array as a bottom surveying tool. This report attempts to quantify problems such as these.

Keywords: Reflection loss – array - beam-forming - ambient noise – simulation - modelling

Contents

1

Introduction

Earlier papers [1-4] introduced and demonstrated an experimental technique whereby bottom reflection loss can be extracted directly from measurements of ambient noise directionality. The process involves simply dividing the up-going sound by the down-going sound at each angle, as measured by a vertical array, and in this respect it is not really an inversion in the usual sense. However if we want to go further than reflection loss as a function of angle and frequency then we do need to search using a geoacoustic search model.

In this paper we are neither interested in inversion nor the processing *per se*, instead we are interested in simulating the data and the process with a view to exploring the limitations of the method. Typically when attempting to understand experimental results one is forced to speculate through lack of knowledge of retrospectively important quantities. This is particularly so if the quantities are difficult or expensive to measure and if the only purpose is to eliminate them from a list of potential sources of error. In this case it may be much easier to investigate the prospective effect by numerical simulation.

The particular points that are addressed here are:

- Foundation of the theory on waves rather than rays

- Effects of uncorrelated noise

- Effects of nearby and distant point sources

- Effects of strong sources received in sidelobes

- Effects of absorption

- Effects of refraction

- Effects of array tilt

- Finite array length effects

- Is the reflection measurement local or is it a spatial average?

In Section 2 we review the simple theory, and then we take the above points in turn and investigate them each as numerical test cases. The results show that the theory is sound, the method is surprisingly robust, and that the measurement is local with a reasonably well-defined 'footprint'.

2

Theory / Background

Noise is measured as a discrete time series on, typically 32, equally spaced vertically separated hydrophones. Frequency-domain beam-forming with some power averaging then results in noise intensity *vs* angle and frequency. Dividing the up-going noise (down-steered beam response) by the down-going (up-steered beam response) we then obtain a power reflection coefficient, and we can map this value from the steer angle at the array to the angle at the seabed. We can mimic this process conveniently using the variant of OASES [5] called OASN. This calculates the cross spectral density matrix $C_{nm}(\omega)$ (at a set of frequencies ω) for a given vertical array in the presence of a surface sheet source and a stratified environment (water column and sediment layers). We then calculate the steered beam response from

$$A(\theta, \omega) = \mathbf{w}^{\mathbf{T}} \mathbf{C} \mathbf{w} = \sum_n^N \sum_m^N a_n a_m C_{nm}(\omega) \exp(-i\omega \tau_{nm}) \tag{2.1}$$

where the τ_{nm} are the steering delays and the $a_{n,m}$ are the shading weights. The mapping from array angle at sound speed c_o to bottom angle at speed c_o is simply

$$\theta_B = \mathrm{acos}(c_B \cos\theta / c_o) \tag{2.2}$$

This estimate of the reflection loss can then be compared with the true reflection loss as calculated by another variant of OASES called OASR. It calculates the plane wave reflection coefficient for exactly the same seabed. Thus we have a self-consistent numerical method of checking the performance of the proposed 'noise inversion' technique; we start with an arbitrary layered environment, calculate the 'true' plane wave reflection loss using OASR, then use OASN and the proposed up-to-down ratio to calculate 'deduced' reflection loss. We can then assess performance of the experimental technique by comparing the two numerical reflection loss results.

In all the following cases we take an environment similar to the sand bottom near the Ragusa Ridge [1,2] with an adjusted layer thickness of 1.3 metres.

3

Test Cases – Isovelocity water

3.1 Addition of uncorrelated noise

Early attempts at deducing reflection loss from noise [3] suffered from seemingly low values of reflection loss. There are one or two possible reasons, one being addition of uncorrelated noise. From Eq (2.1) it can be seen that uncorrelated noise enhances the diagonal of C_{nm} and results in the same addition to beam response for all steer directions. Thus the up-to-down ratio U/D becomes (U+a)/(D+a) and is contaminated by the addition. The solution will tend towards unity (or reflection loss tends to 0 dB). As will be seen later, a similar effect can be had from the side lobes of a dominant noise source such as distant shipping.

3.2 Isovelocity: no absorption

Both analytical and numerical calculations fail when there are no losses at all because of a two-dimensional version of Olbers' paradox [6]. In short, a sheet source carries on making contributions for ever-increasing ranges in a cylindrical environment if there are no losses.

Nevertheless it would be desirable to run a case where there is bottom reflection loss but no absorption in the water. This is difficult to achieve with OASN, but for completely different reasons, as follows [7]. In OASES and OASN the solution depends on numerical integration (actually an FFT) in wavenumber space in which the resonance of each loss-free mode resembles a delta function. To get around the numerical integration problem, absorption is deliberately introduced before the integration to widen these resonance features. (Actually the integration is taken along a line slightly displaced from the real axis.) The resulting function of range (in the propagation loss version, OASES) is compensated for the artificial loss with an exponential growth. However in the noise model (OASN) it is still possible to offset the line of integration from the real axis, but it is not possible to compensate with an exponential growth because there is no particular range associated with the noise source, it is a sheet. One option is to increase the FFT resolution, but there are still practical problems. The alternative is to insert only uncompensated real absorptions.

3.3 Isovelocity with volume absorption – sheet source

3.3.1 Beam response

Figure 1 shows simulated beam response for a 32-element VLA using OASN with isovelocity water and absorption following [8]. Detailed parameters are given in Table 1.

Table 1 *Environmental parameters*

| Layer description	Layer thickness (m)	Sound speed (m/s)*	Attenuation (dB/λ)	Specific gravity
Water column	130	1517	Ref [8]	1
Sediment layer	1.3	1554	0.14	1.88
Subbottom	∞	1643	0.14	1.88

* Note that the geoacoustic parameters remain the same for all simulations, while the sound speed profile is modified in Section 4.

Note that the geoacoustic parameters remain the same for all simulations, while the sound speed profile. Throughout this report negative angles correspond to upward pointing beams that collect downgoing noise.

It is shown in [6] that a predominantly volume-absorbing environment results in noise directionality being proportional to $\sin^2(\theta)$. So Fig. 1 is doing what we expect from the theoretical point of view since, even with significant bottom losses, at low enough angles and high enough frequencies the dominant loss in a ray cycle is volume absorption. Before looking at the deduced reflection loss it is interesting to compare the plot with experimental beam responses. Figures 2 and 3 show equivalent pictures for, respectively, an isovelocity case (muddy bottom near Elba [1]), and a downward refracting case (sandy bottom south of Sicily [1]). Figure 3 has an equivalent weak response in the horizontal, but this is a 'noise-notch' caused by downward refraction [6]. In contrast the isovelocity case (Fig. 2) shows a clear peak at horizontal. The ray theory of [6] assumes dipole sources; OASN takes finite depth point sources which act like dipoles if closer than a fraction of a wavelength to the surface or monopoles if deeper. The source depths in OASN were taken to be one third of a wavelength. In short, both ray and wave theory predict a 'hole' in the middle which suggests that the distant sources seen experimentally in Fig. 3 are not dipoles. In fact a plausible explanation is that they are contributions from many distant ships whose source depth may be several wavelengths. Typically in noise studies one takes the source depth for a ship to be 5 metres [9]. However this does not rule out the possibility of deep wind or bubble plume sources.
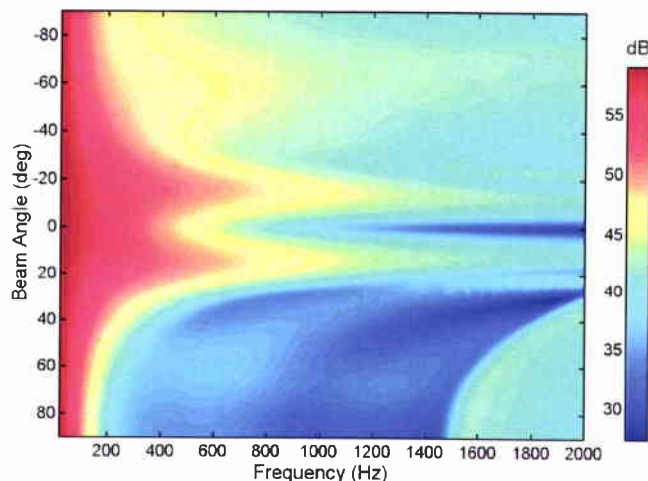
Figure 1 *Simulated beam response for a 32-element VLA in isovelocity water using OASN. Note that negative angles are upward pointing beams that collect downgoing noise.*
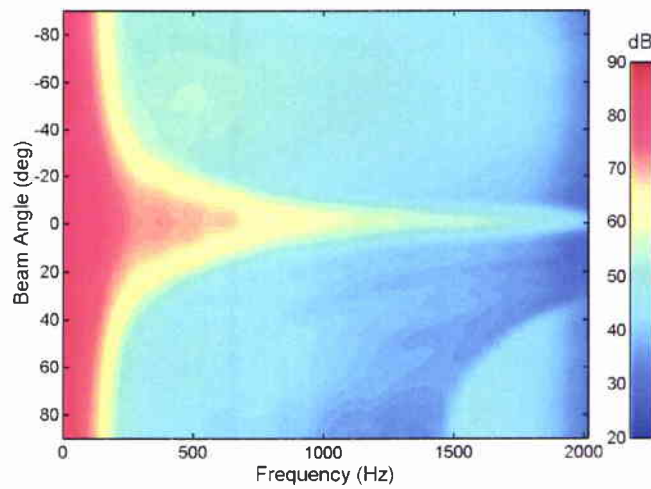
Figure 2 *Experimental Elba mud showing peak of noise at horizontal in isovelocity conditions.*
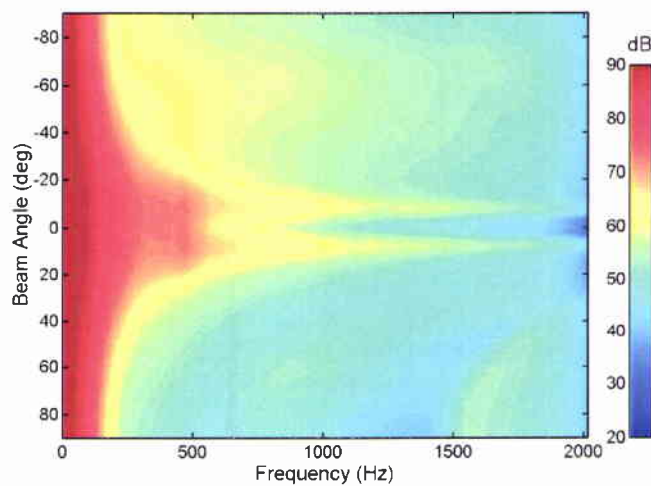

Figure 3 *Experimental Sicily sand showing noise notch – absence of noise at small angles caused by downward refraction.*

3.3.2 Reflection Loss

In reality, whether the distant ships or distant wind behave like a dipole or a monopole makes no difference to this experimental technique; it simply relies on an input noise directionality with sources on or near the sea surface. Likewise, absorption in the water column is unimportant. Inserting the geoacoustic parameters of Table 1 into OASR we obtain the 'ground truth' plane wave reflection loss vs angle and frequency (Fig. 4).
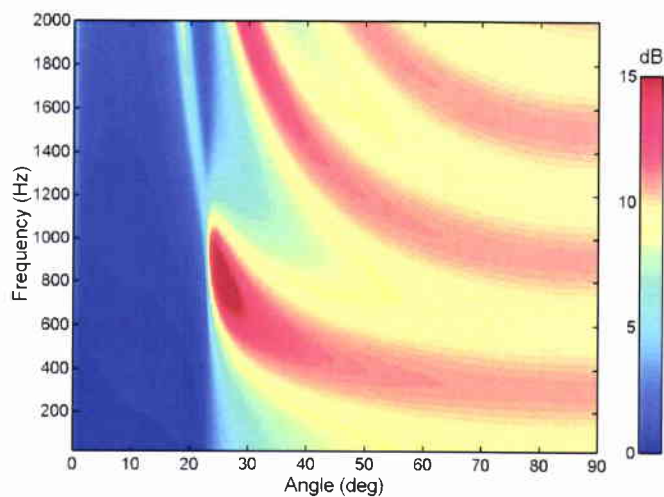
Figure 4 *'Ground truth' plane wave reflection loss from OASR using Table 1 parameters.*
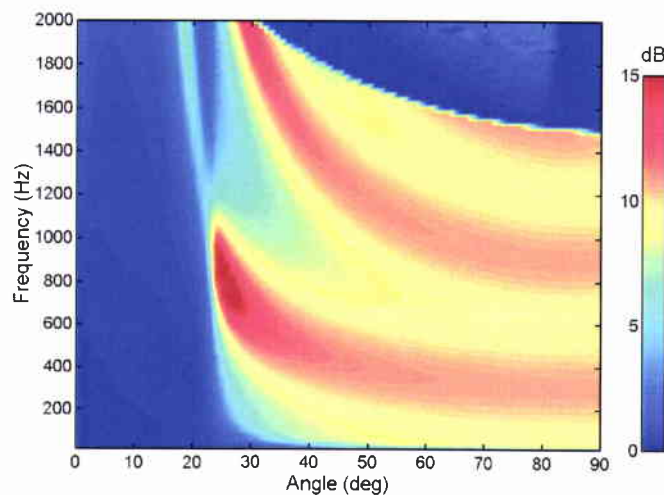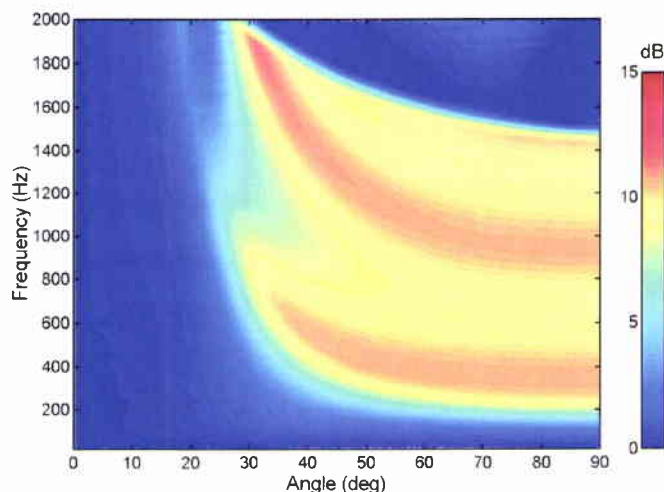

Figure 5 *Up-to-down beam ratio resulting from running OASN for a full water depth array (275 hydrophones still at 0.5 m spacing).*

Features to note in this plot are the main critical angle at 23° (corresponding to the bottom half-space speed), interference fringes at steeper angles (with frequency separation depending on layer thickness and depth of modulation depending on impedance contrasts), and a weak fringe in the angle range between 23° and the sediment layer critical angle (13°).

The up-to-down beam ratio resulting from running OASN for a full water depth array (275 hydrophones still at 0.5 m spacing) is shown in Fig. 5. Comparing this with the 'ground truth' (Fig. 4) we see a difference for high frequencies and high angles and a minor difference in the vicinity of 30°, 50 Hz. However the rest is near perfect agreement, including critical angles, fringe positions, fringe depth of modulation, and strength in the angle regime below the critical angle. The high frequency difference is easily explained since it is the result of exceeding the design frequency of the vertical array. Beyond this

SACLANTCEN SM-392

point the beam pattern can form grating lobes[1], and in particular, a downward steered beam sees direct contributions from upwards through the grating lobe. This phenomenon can be seen in all the experimental and simulated array response curves (eg Figs 1-3) as the light coloured arc (following $f \times (1+\sin\theta_s) = $ const) that reaches 90° at 1500 Hz (the design frequency for an array with hydrophones at 0.5 m separation).

Simulation for the same configuration array as in the experiments (32 elements at 0.5m separation, deployed at approximately mid-depth) is shown in Fig. 6.

Figure 6 *Up-to-down beam ratio resulting from running OASN for a 32 element array at 0.5 m separation.*

Now we see the effects of the poorer angle resolution, and the results are very similar to the experimental ones of [1]. Comparing with Figs 4,5 the thin fringe and the peak loss near 20° are lost, or at least, smoothed over. The grating lobe is unchanged, since the hydrophone separations are the same as before. The most important difference is the gap that has opened up below 200 Hz; this feature was present in Fig. 5 but negligibly small. It is a direct result of the frequency-dependent beam width. The up-to-down ratio of near horizontal beams tends to unity (0 dB) for angles from zero up to the angle resolution. It is already clear from the beam response that angle resolution is progressively poorer at lower frequencies, in fact by 150 Hz the resolution is worse than a radian. So the anomalous low loss region at the bottom of Fig. 6 mimics the shape of the array response. It is possible to improve performance in this region by using adaptive beam-forming, but this will not be pursued here.

3.4 Isovelocity with volume absorption – distant point source

What we are trying to simulate here is sources that cannot be regarded as a spatially slowly varying sheet, for instance, individual ships or groups of ships in no specific arrangement. A problem with simulation is that the point source calculation needs to be coherent in order to retain important propagation features (and some credibility), but this

---

[1]A grating lobe is as powerful as the main lobe but exists at an angle determined by
$Nka(\sin\theta - \sin\theta_s) = m\pi$, where θ_s is the desired steer angle, N is the number of hydrophones at separation a, k is the wavenumber, and m is an integer (+/- 1 in this case).

imposes fine structure in frequency and angle. In this example (Fig. 7) with point source at 20 km the scale of the structure is of order 10 Hz and 1°.
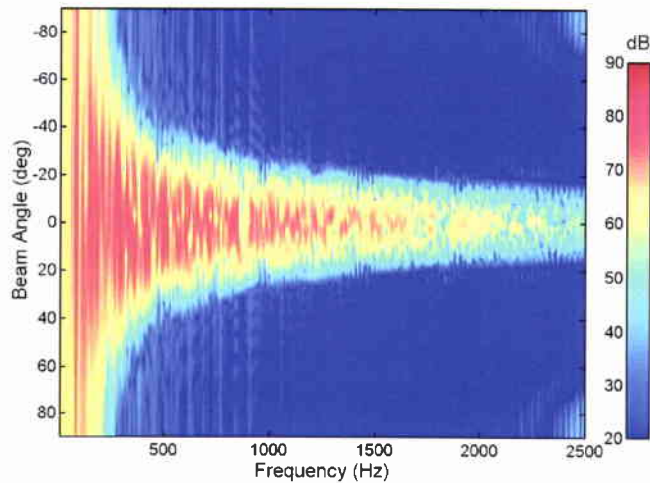

Figure 7 *Beam response from a distant point source with no averaging.*

In reality this would be smoothed out by temporal fluctuations in the propagation, motion of the ship, finite length of the ship, and depth spread of the ship. Figure 8 shows a running-frequency-averaged version (source level 150 dB re 1 μPa @ 1m, bandwidth equals one tenth of frequency).
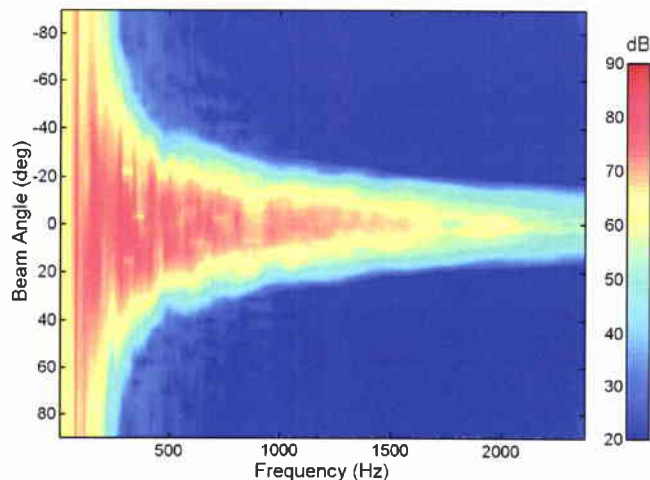

Figure 8 *Beam response from a distant point source with frequency averaging.*

It is clear that the distant ship supplies noise within the critical angle but hardly anything outside. Therefore we would not expect a complete reflection loss plot with ships alone although the remaining low angle part ought to be correct. A more interesting result is given by combining the ship with sheet noise. In Fig. 9 we see the beam response for white sheet noise with a source level of 65 dB re 1 μPa @ 1m per m^2 .
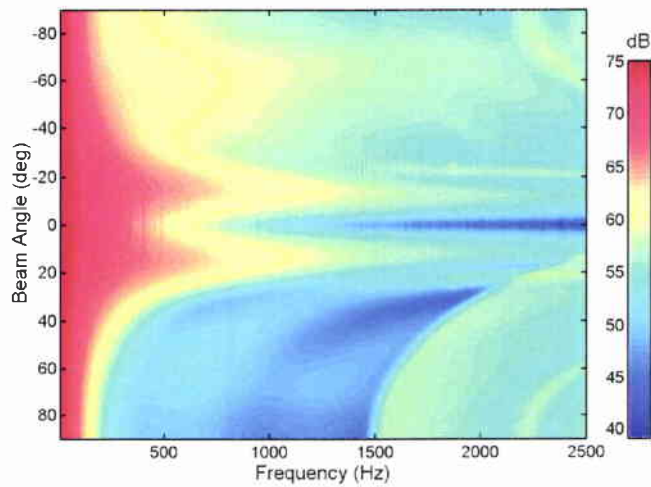
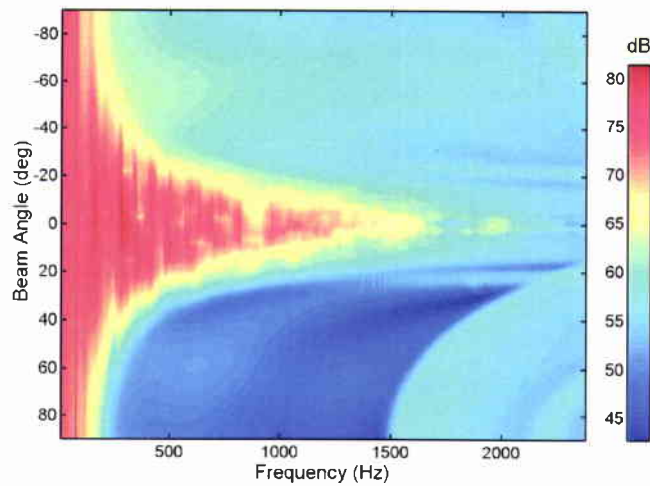**Figure 9** *Beam response from a sheet source.*
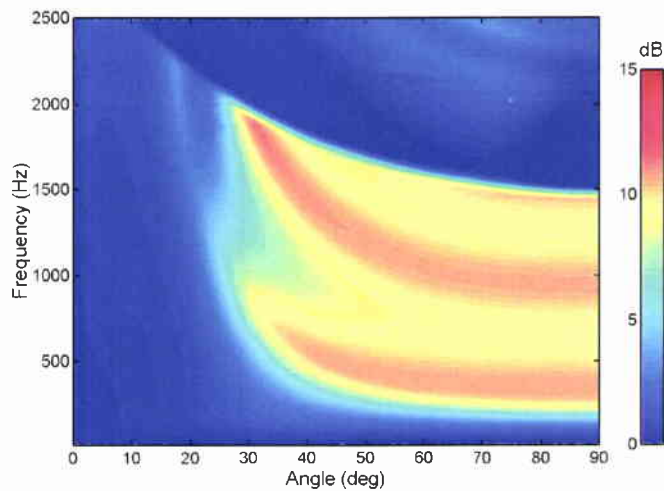
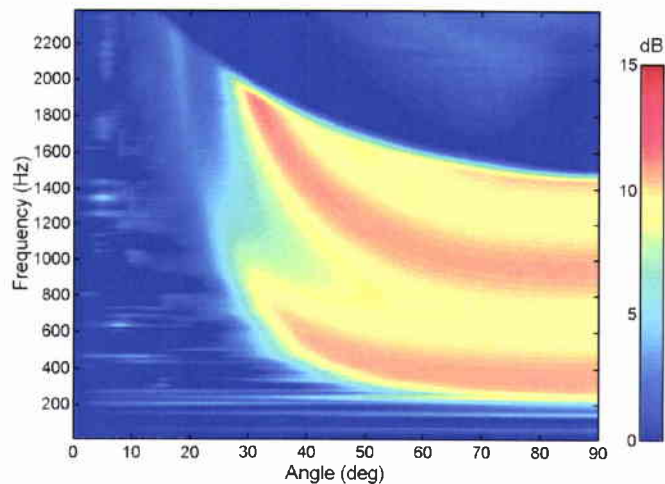**Figure 10** *Deduced reflection loss from noise alone.*

For completeness the deduced reflection loss is shown in Fig. 10. Combining point and sheet noise we obtain the beam response shown in Fig. 11. This bears a remarkable resemblance to the experimental plots, eg Fig. 2.

Finally we plot the deduced reflection loss in Fig. 12. Comparing this with Fig. 10, as we might expect, there are chaotic features below 20° and at low frequencies where the ship tends to dominate. Of course, the proportion of ship to wind is an important quantity for several reasons, the most important of which is that upward and downward beams may be contaminated by the sidelobe returns from strong horizontal shipping returns. This weakens the contrast of the interference fringes. Otherwise the addition of distant shipping has no adverse effects.

Figure 11 *Beam response from combination of distant point source and sheet noise source.*


Figure 12 *Deduced reflection loss from combination of distant point source and sheet noise source.*

3.5 Isovelocity with volume absorption – nearby point source

For the coherence reasons discussed above it is even more difficult to simulate nearby sources. However our usual main reason for simulating is to be certain that we have a well defined problem before interpreting the results. In the case of a nearby source, documented experimental examples exist where we do know the position and number of ships. Therefore we can use these in preference to simulations in this case. Here we examine the case of a fishing boat within 100m of the array followed within minutes by a very large ship within 1 km or so. Both events were seen and logged on radar, and the pictures shown below were available in real time. The full sequence is assimilated most easily as a movie.

The main relevant effect of a nearby point source is to provide resolvable eigenrays. Since generally these are placed asymmetrically about horizontal an instantaneous ratio of up-to-down no longer works. Nevertheless a time average or a more sophisticated treatment of the time-varying angles could still reveal the bottom loss. An alternative is to deliberately degrade the resolution to force eigenray overlap.

SACLANTCEN SM-392

Figures 13 and 14 are selected 10-second averages of noise and their respective deduced reflection losses. Figs 13 (a,b) are before the events (time code included in title vla*yyyydddhhmmss*). Fig. 13 (c,d) is the approach of the fishing boat, and Fig. 13 (e,f) is the closest point of approach (CPA). One can clearly see the strong upward direct path at about 16° and the single bottom reflected paths at about 59° up and 49° down. As an aside, it is possible (redundantly) to calculate from the array depth of 50m that the CPA range was 174m (suspiciously close to the distance between the array and the radio buoy!). One can also calculate the water depth as 2.7×(array depth) = 137m. The reflection loss pictures show how, without any extra processing, the eigenrays interfere with the result.
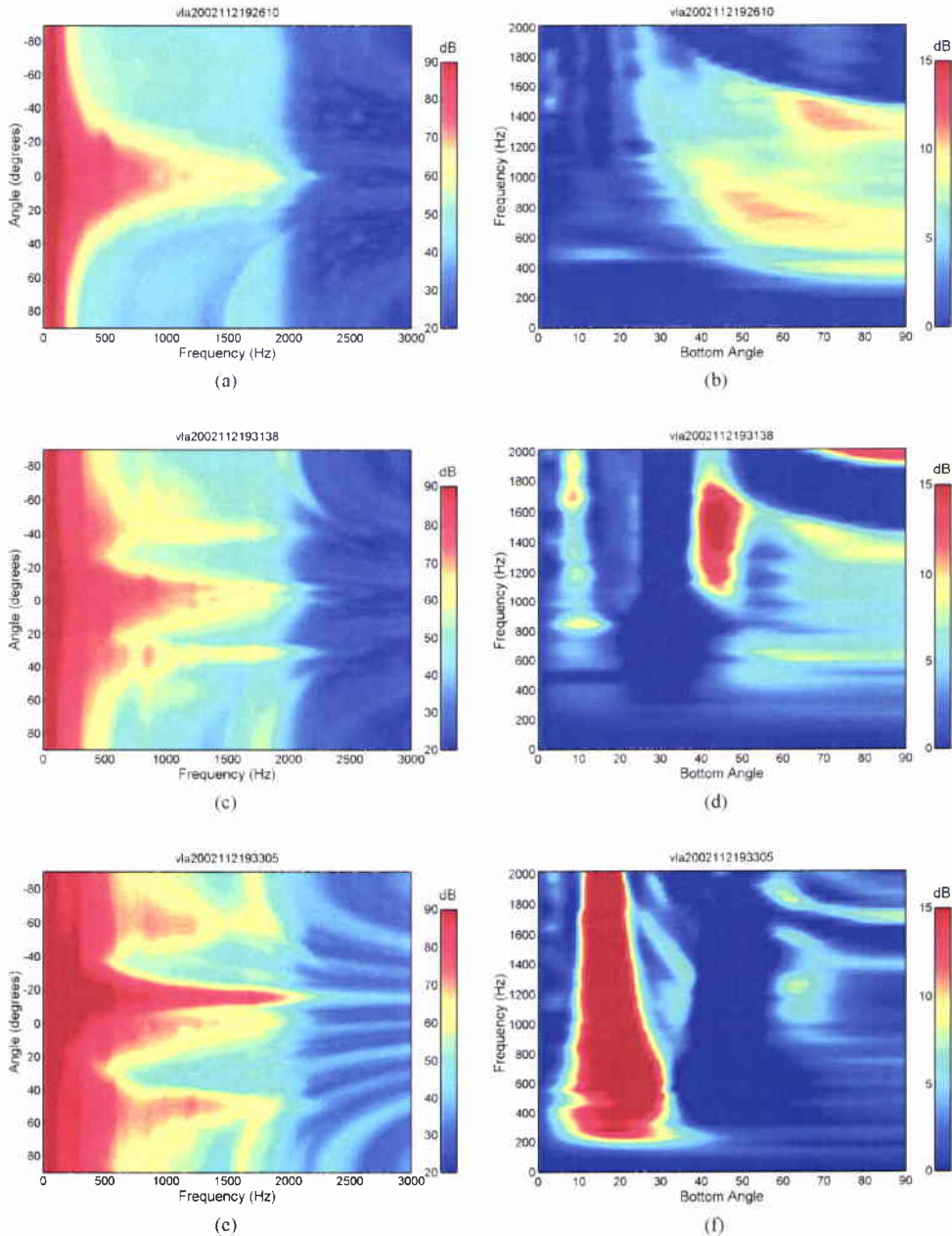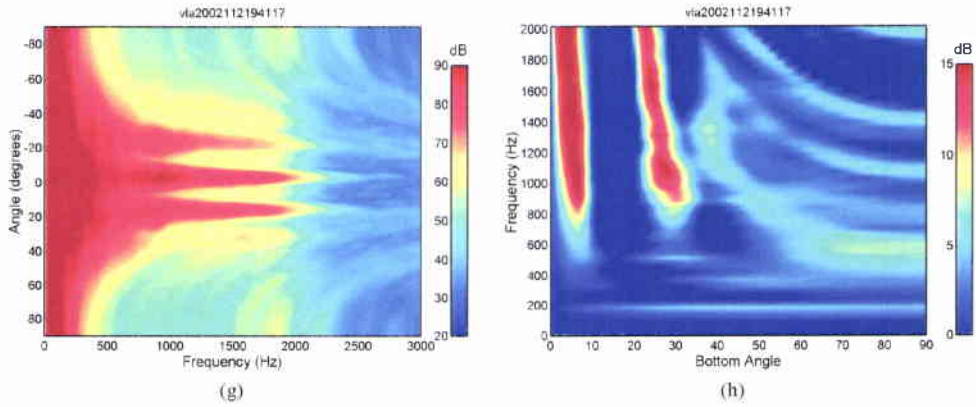

Figure 13 *Beam response and derived reflection loss: (a,b) no ships, (c-f) nearby fishing boat. Note time code in title. CPA is (e,f).*

A similar sequence for the approach of a large ship is shown in Fig. 14(a-h) with the last pair at CPA. Again using the eigenray separation we can calculate the range in the first case as 1.6km and in the CPA case as 800m! In this case the data are unusable for about 7 minutes on either side of CPA, however devising a general rule is impossible, and the usual problem is the background shipping level compared with the wind strength rather than individual ships.

(a)

(b)

(c)

(d)

(e)

(f)
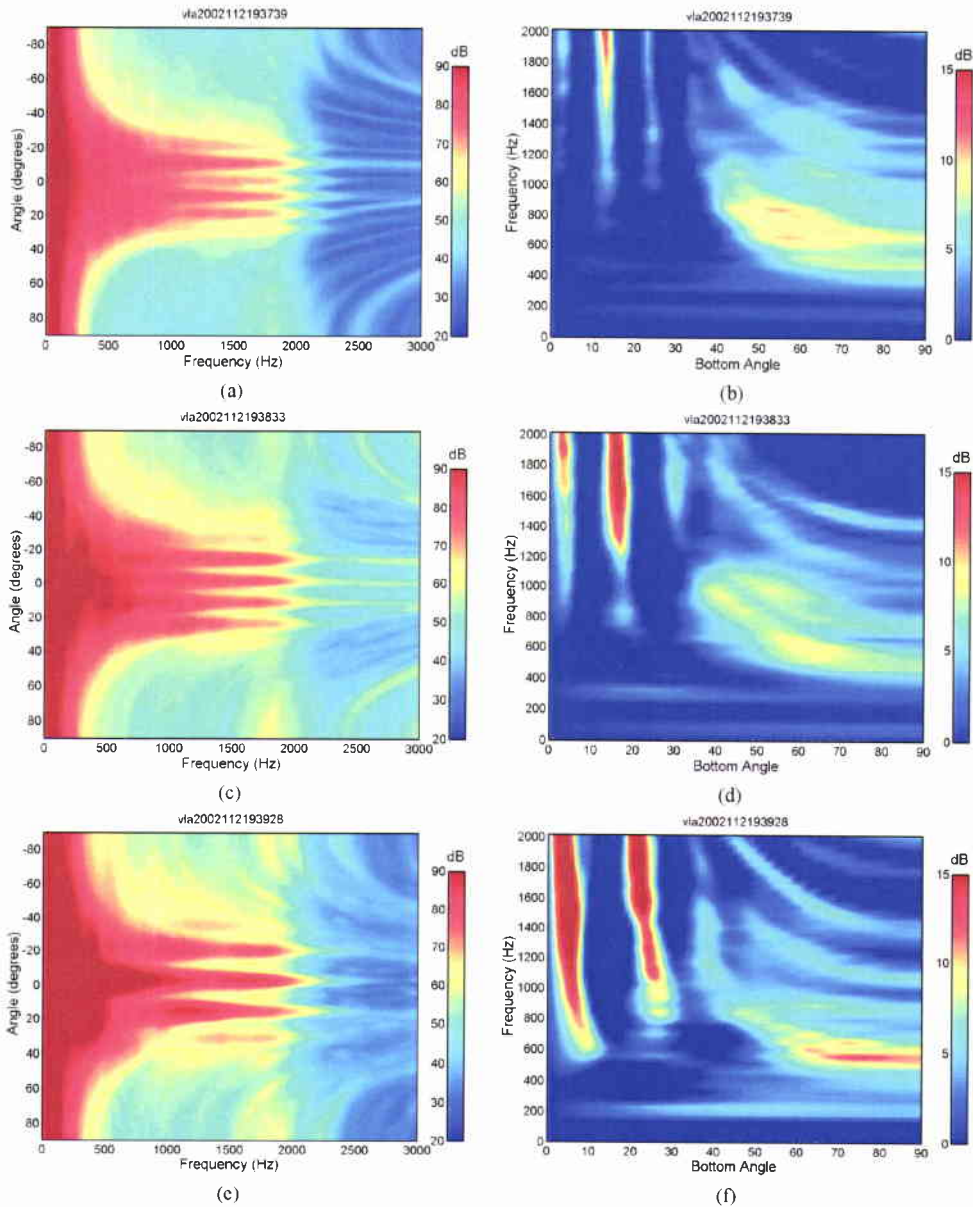
Figure 14 (continued on next page) *Beam response and derived reflection loss with large ship approaching. Note time code in title. CPA is (g,h).*

SACLANTCEN SM-392

(g)   (h)

Figure 14 continued *Beam response and derived reflection loss with large ship approaching. Note time code in title. CPA is (g,h).*

4

Test cases – Refracting environment

Simple ray theory for a small array [6] (ie, small compared to the water depth) suggests that the sole effect of refraction is to convert the true reflection angle at the seabed into a measured angle at the array. These angles are related by Snell's law. In addition the noise directionality itself is affected by the sound speed profile above the receiver, and it is possible that there may be a "noise notch" [6]. Nevertheless the angles for which we have measurements map on to angles at the seabed. From a numerical point of view this simply means that a change of angle axis annotation on the plots to a non-linear position of ticks (θ_b = acos(cosθ_r c_b/c_r) is sufficient. The purpose of this section is to demonstrate numerically, using a wave solution, that this is indeed true.
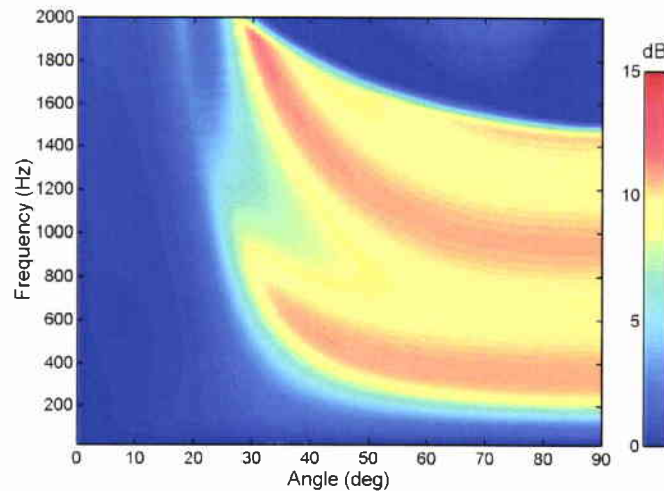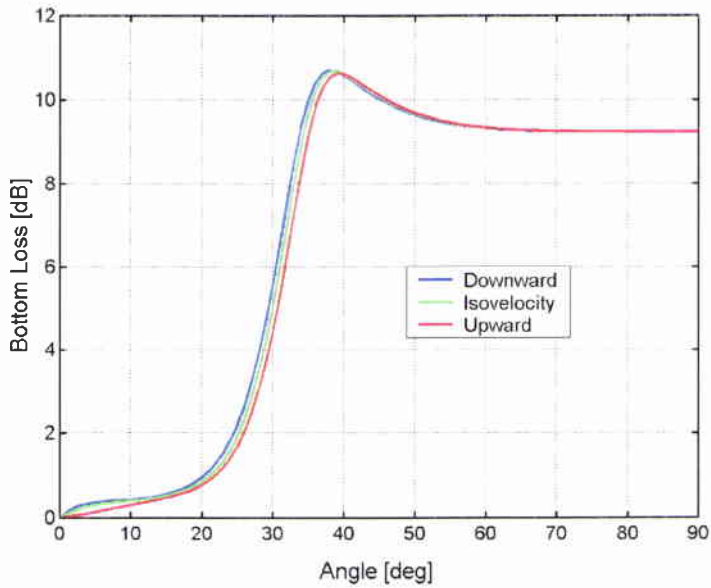

Figure 15 *Deduced reflection loss with downward refraction.*

In these numerical experiments it is important to remember that the 'ground truth' OASR plane wave reflection loss is also slightly affected by the sound speed profile in the water (not just the sound speed value immediately above the bottom). We consider three linear sound speed profiles all with the array at mid-depth, 1512m/s at the sea bed: downward refraction (1522m/s at the surface), isovelocity (1512m/s at the surface), and upward refraction (1502m/s at the surface). Figure 15 is for the downward refraction case. Comparing it with Fig. 6 (isovelocity) it is impossible to see any difference by eye. We actually expect 0° at the array to map to 4.65°, but there cannot be any surface generated noise at the array (other than diffraction effects) at array angles less than (by coincidence) 4.65°. This surface ray reaches the seabed at 6.57°.

It is easier to inspect the differences with a line graph at a single frequency. Figure 16 shows the three curves without any angle correction. That is, OASN provided the cross-spectral-density, and this was plane wave beam-formed to a uniform spread of angles *at the receiver*. In contrast, in Fig. 17 the same function is plotted against angle *at the seabed*. In the downward refraction case the line hits 0 dB at about 4.5° as we expect. The isovelocity line is, of course, unchanged. In the upward refraction case there is a range of

angles at the receiver that never reach the bottom ($-4.65° < θ_r < 4.65°$), and $0°$ at the seabed corresponds to $4.65°$ at the array. The angle-corrected curves are extremely close to each other. Figure 18 shows the 'ground truth' plane wave reflection loss from OASR. The small differences between upward and downward refraction are also seen here because the environment still includes the water column. The rather larger differences between OASR (Fig. 18) and OASN (Fig. 17) have been seen earlier and are caused by the smudging effect of beamforming.
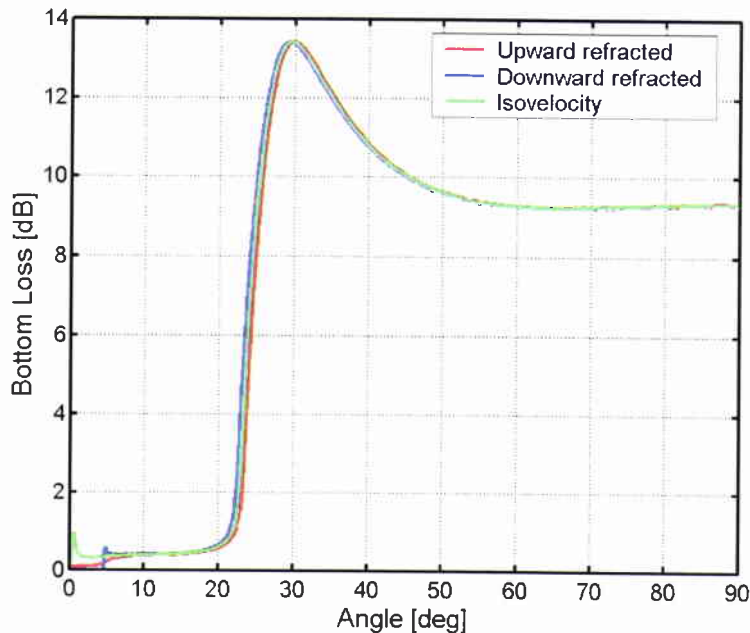

Figure 16 *Reflection loss at 600 Hz with downward refraction, upward refraction and isovelocity plotted against angle at the array.*
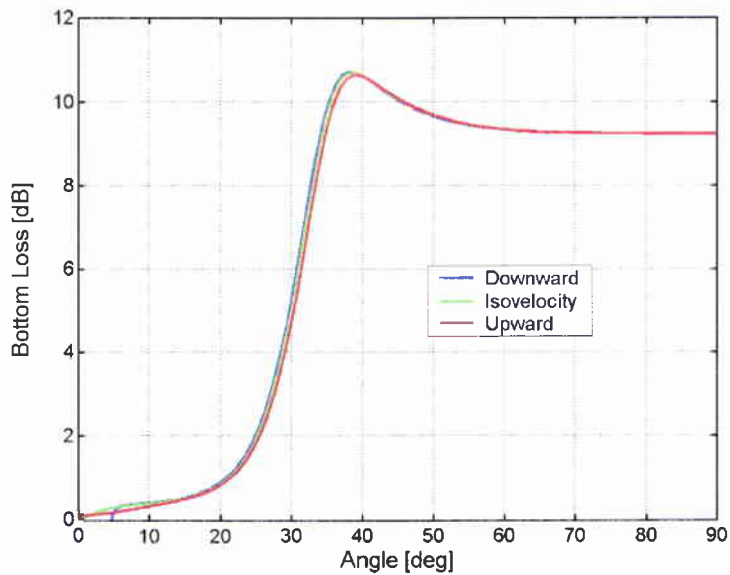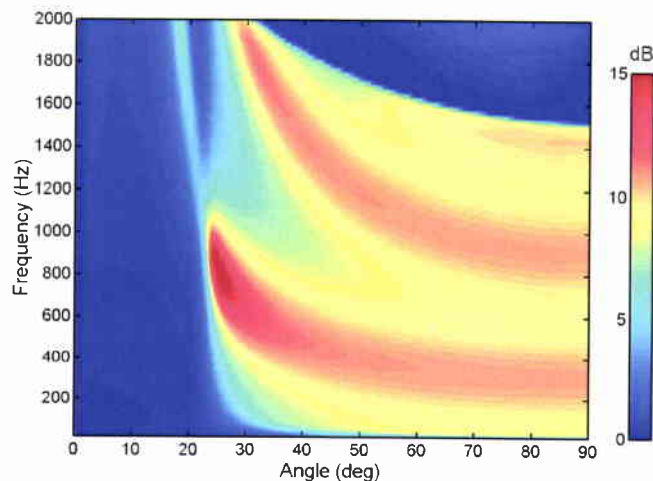

Figure 17 *Reflection loss at 600 Hz with downward refraction, upward refraction and isovelocity plotted against bottom angle.*

The effect of lengthening the array to the full water column in a downward refracting environment is shown in Fig. 19. Comparing this with the isovelocity case (Fig. 5) again we barely see any change at all. One might have expected the beam-forming to be spoilt by the variation in sound speed along the array, but apparently the effect is insignificant.

Figure 18 *'Ground truth' plane wave reflection loss still including the SSP, ie downward refraction, upward refraction and isovelocity plotted against bottom angle. Notice that the lines are not in absolutely perfect agreement*

Figure 19 *Deduced reflection loss with downward refraction and a full water depth array*

5

Test cases – Array tilt

5.1 Tilted array – sheet source

Using conventional beam-forming tilting the array has surprisingly little effect on the beam response and the deduced reflection loss. A progression is shown for tilts of the 16m array of 1°, 3°, 5°, 10°, 15° in Fig. 20(a-j). Hardly any effect at all is visible up to 5° in the reflection loss, except for a slight weakening in the intensity contrast. Changes become more visible at 10°, and then finally at 15° there are serious changes. This is not surprising as the tilt is comparable with the lobe separation in the beam response. Nevertheless the reflection still retains the main features of the vertical case.

The reason for this lack of sensitivity is probably that the visual impression one gets is largely from the high angle interference pattern, and the tilts are relatively small angles. In addition the interference structure is mainly a function of frequency and changes rather slowly with angle. Therefore any angle smoothing or smudging associated with the tilt (remember that an upward tilt in one direction is a downward one in another) has very little effect.
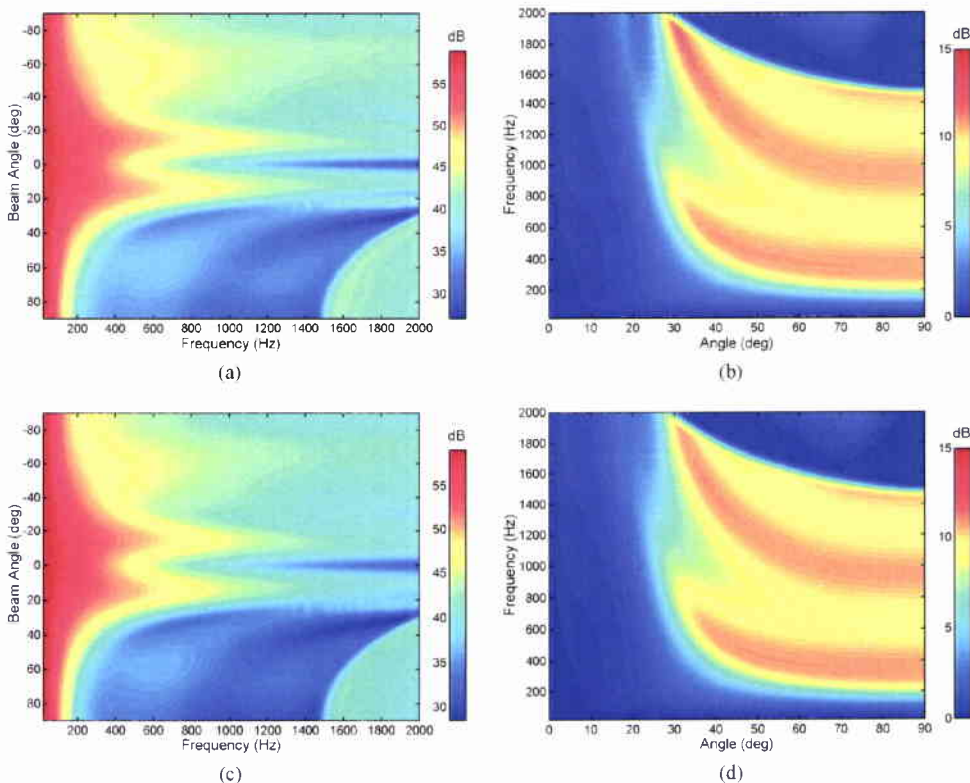
Figure 20 (continued on next page) *Pairs of beam response and deduced reflection loss for short array tilts of 1° (a,b), 3° (c,d).*

(e)

(f)

(g)

(h)

(i)

(j)
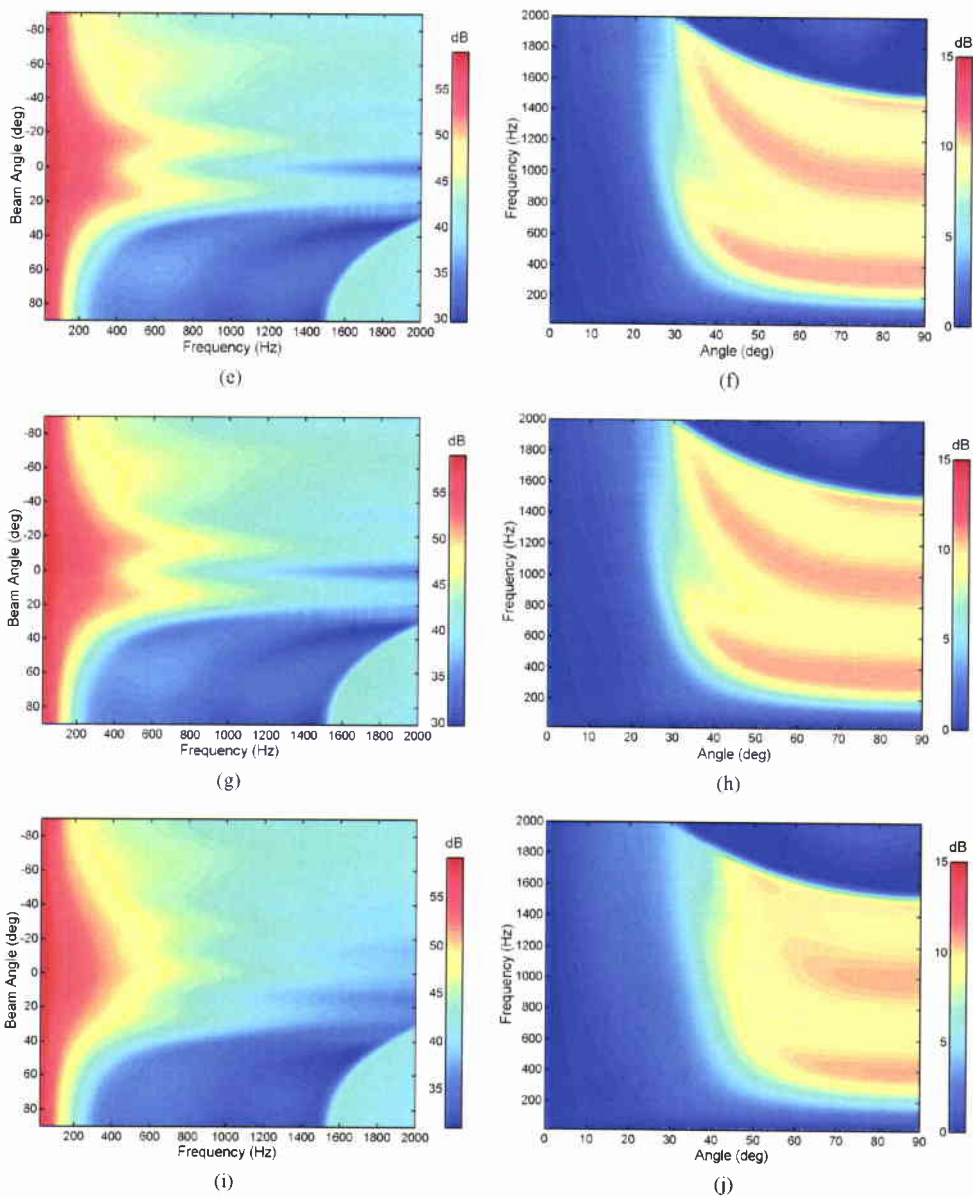
Figure 20 continued *Pairs of beam response and deduced reflection loss for short array tilts of:*
*5°(e,f), 10°(g,h), 15°(i,j).*

If we extend the array to the full water depth before tilting it we find equivalent results in
Fig. 21(a-h) for tilts of 1°, 3°, 5°, 10°. The pictures are more quantised because of
computation time problems. On the whole the long array is naturally more sensitive to
angle changes, but still the representation of reflection loss is very good even at 10°.

5.2 Tilted array – combined point and sheet source

In these examples the array tilt is always 5° in the North-South/vertical plane, with the
bottom of the array shifted towards the N. As well as the sheet source of Section 3.4 there
is now a point source at various bearings but always 20 km from the receiver. Figure
22(a-h) shows pairs of beam response and reflection loss for source to the N, E, S, W.

SACLANTCEN SM-392
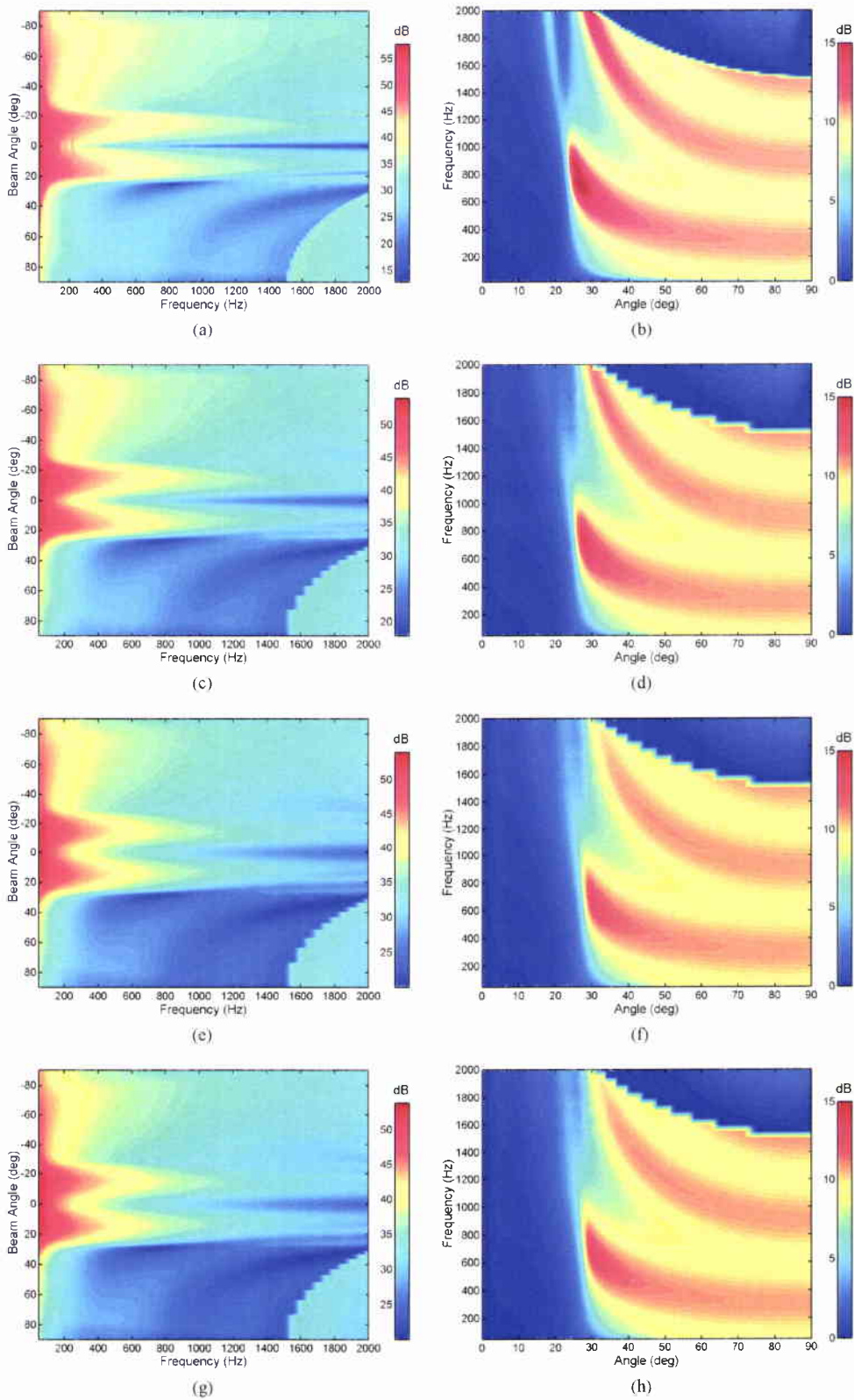
Figure 21 *Pairs of beam response and deduced reflection loss for long array tilts of: 1° (a,b), 3° (c,d), 5° (e,f), 10° (g,h).*
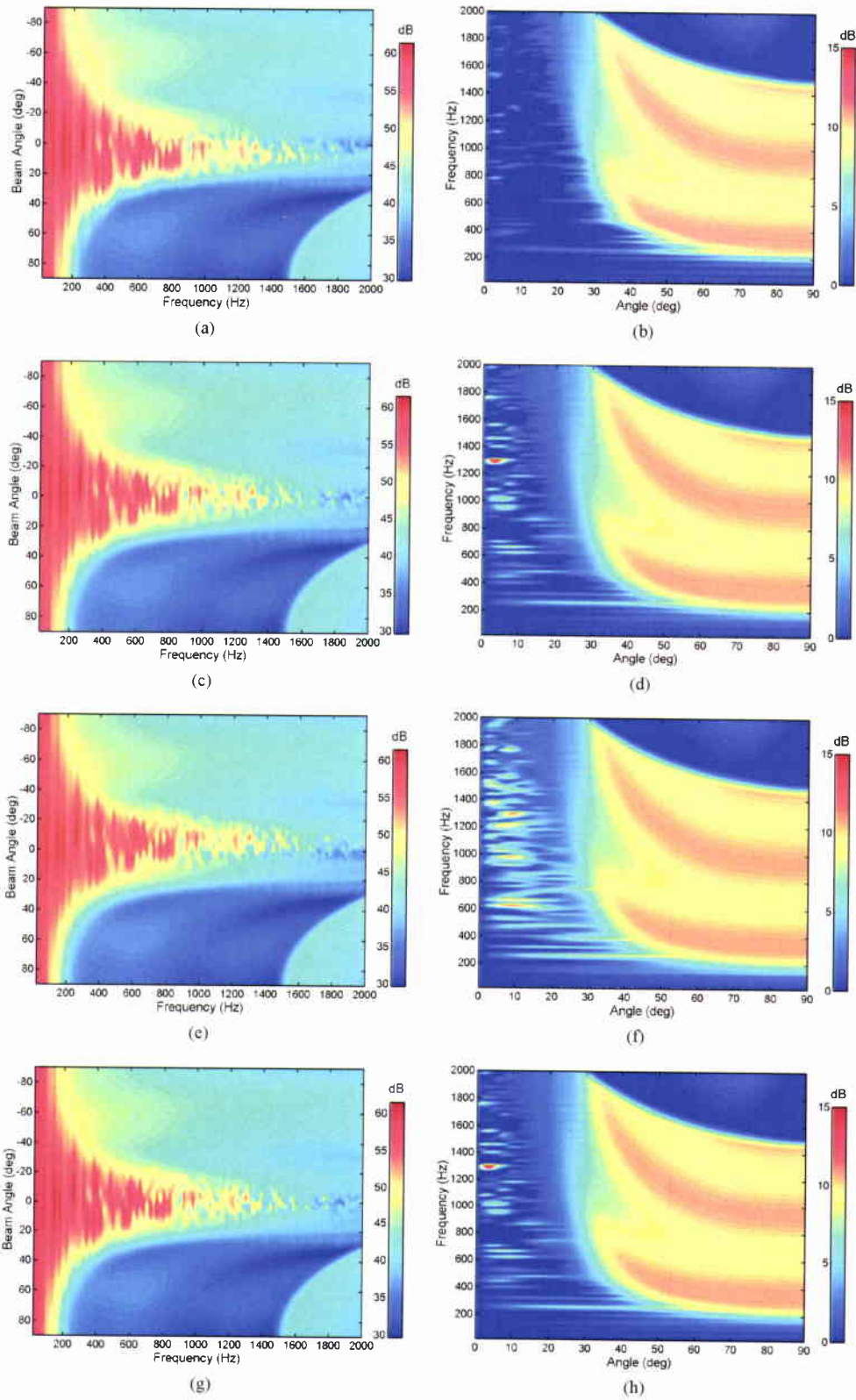
Figure 22 *Pairs of beam response and deduced reflection loss for short array tilted at 5° (bottom towards N) with both sheet and point source at 20 km to the North (a,b), East (c,d), South (e,f), West (g,h).*
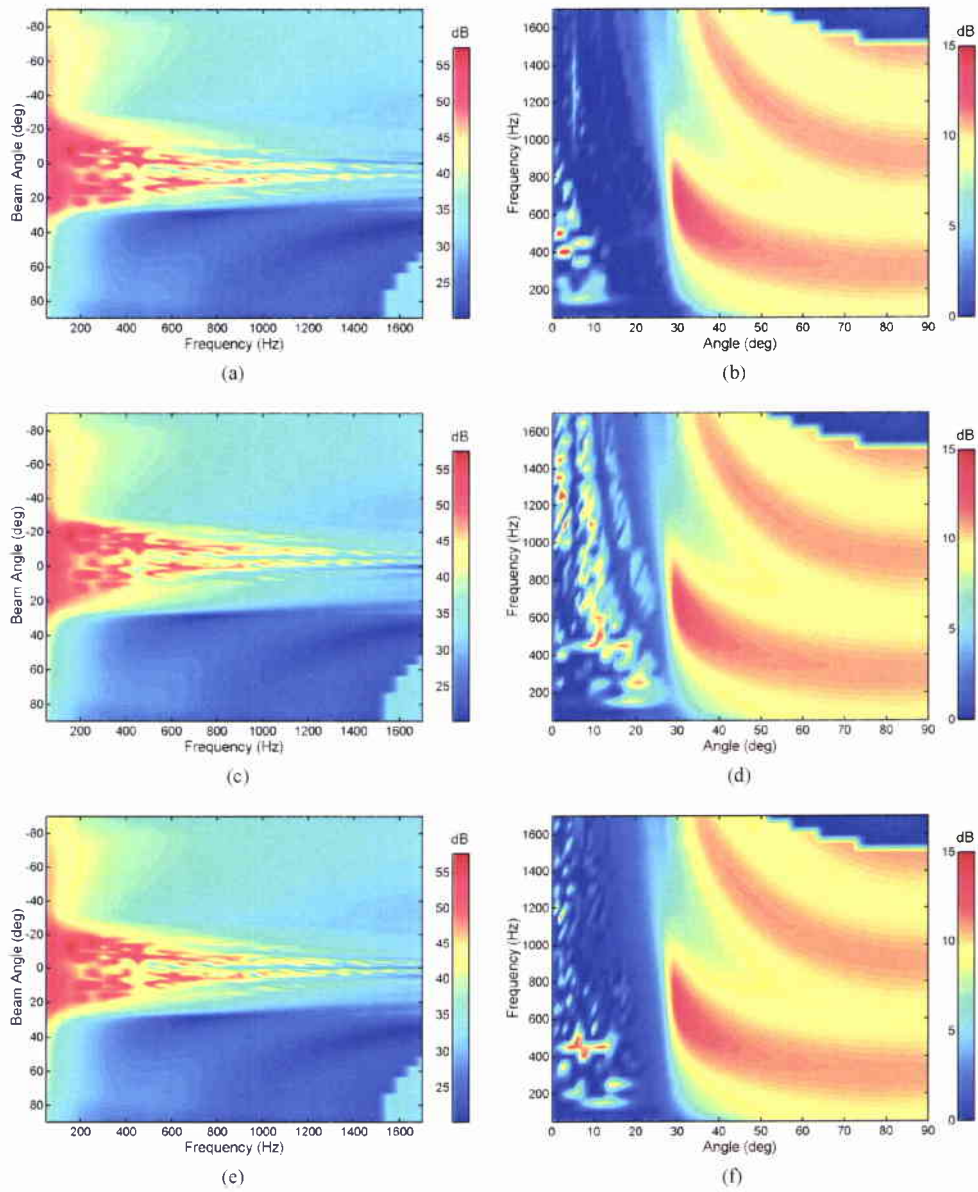
Figure 23 *Pairs of beam response and deduced reflection loss for long array tilted at 5° (bottom towards N) with both sheet and point source at 20 km to the North (a,b), South (c,d), West (e,f).*

6

Test cases – Range-dependence

6.1 Where is the reflection point? Test case theory

An interesting question is, where is the reflector whose strength we are measuring? Is it near the array, or is it some kind of average over great distances? After all, the theory, whether ray or mode, postulates noise sources out to infinity whose contributions combine to give the coherence we receive. If the reflector is near the array then this technique can be used for surveying. To explore the possibilities we need a range-dependent model in which we can locally change the bottom properties. This is a tall order because, at the same time we require fidelity at high angles and short ranges. This rules out discrete spectrum normal mode programs such as C-SNAP[10], and it also rules out many parabolic equation models. However the range-dependent PE model RAM [11] appears to be able to handle all three problems.
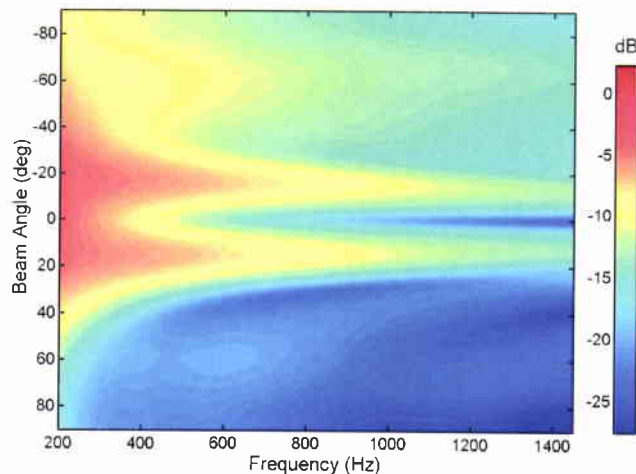

Figure 24 *Beam response to a sheet of noise sources using RAM. This can be compared with the OASN plot in Fig 1. Note restricted frequency range for RAM. Agreement is good.*

Figure 24 is a plot of the array response to sheet noise using RAM. It can be compared directly with the OASN version in Fig. 1. The hydrophones are modelled as sources, and RAM's marching-in-range solution contains intensity at all depths including a fraction of a wavelength below the surface where our noise sources are located. Thus by swapping sources and receivers (as allowed by reciprocity) RAM provides the correlation matrix at the VLA from which we can calculate the steered beams as usual.

In this numerical experiment, as shown in Fig. 25 [4], we create a variable radius circular area of seabed beneath the array with three layers as before (environment E1), outside which the bottom is a simple half-space (environment E2), thus providing distinguishable bottom properties (E1 creates interference fringes; E2 does not). We use the range-dependent model RAM with swapped sources and receivers to provide the correlation matrix at the VLA.

Assuming that the ray interpretation is correct we expect to see a transition from E1 to E2 when the steer angle points directly at the edge of the E1 disk. Of course diffraction effects and the finite size of the array will blur this transition. By changing the diameter of the E1 disk we can find the "footprint" of the array. This is the diameter where the result is in clear transition between the entirely E1 environment and the entirely E2 environment.
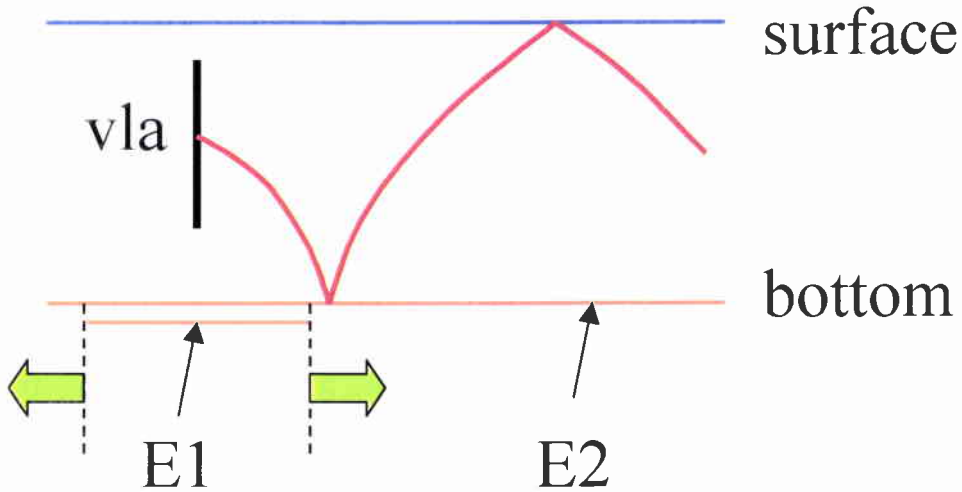
Figure 25 *Three-dimensional geometry for RAM numerical experiment showing incoming path bouncing either in bottom environment E1 (a disk of 2-layer sediment) or environment E2 (a 1-layer sediment). By changing the diameter of the E1 disk one expects to "deduce" bottom properties of either E1 or E2 if we believe the ray hypothesis.*
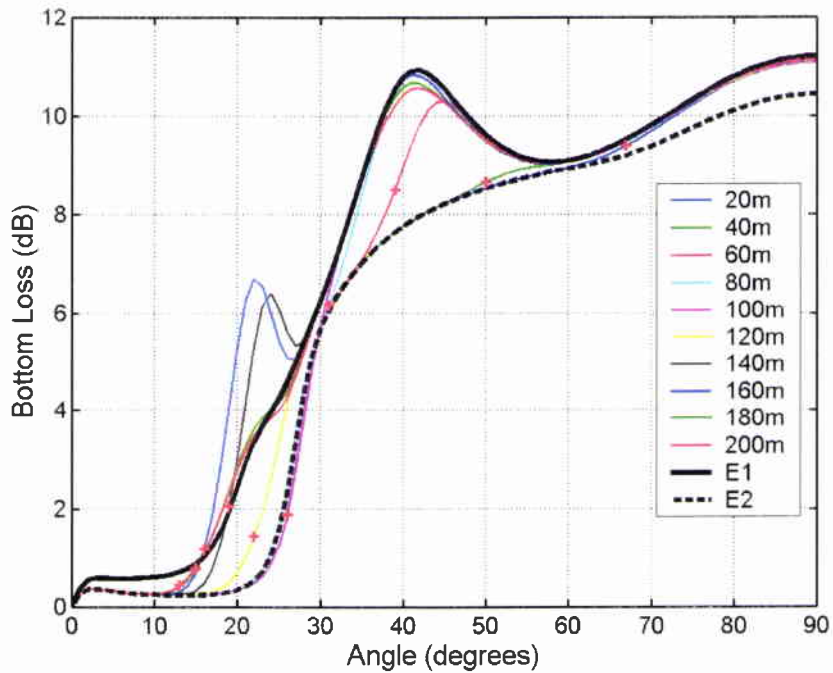
6.2 Isovelocity at two frequencies
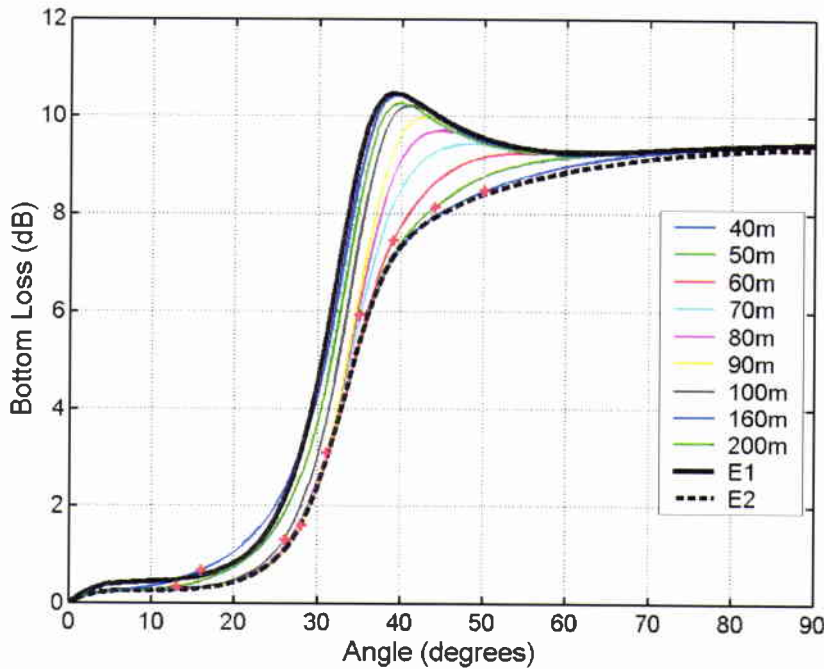
Figure 26 *Deduced bottom loss at 600 Hz (colour-coded lines) for various sizes of bottom disk with E1 properties (three-layer, giving resonance peak), outside which there is E2 properties (two-layer, standard Rayleigh). Red crosses indicate the angle for each coloured line at which we expect a rough transition from E2 to E1 (black lines).*

Figure 26 is a slice through the earlier style of plot at one frequency (600 Hz). The two thick black lines correspond to extremely large bottom disks of respectively environments E1 and E2; E1 can be recognised by its resonance peak, and E2 is a simple Rayleigh shape. In between are coloured lines corresponding to different radius E1 environment, and the red crosses on each line mark the steer angle to the disk edge, as seen from the centre of the array. (As a cross-check for identifying the coloured lines and their red crosses, the shortest radii go with the largest angles). If we inspect each line in turn we find that for angles greater than that of the cross (angles nearer the vertical) the curve tends to the E1 thick line. Conversely for shallower angles the curve tends to the E2 thick line. This demonstrates with a full wave model that the reflection loss we deduce really is that of the area within about one fraction of a ray cycle from the array (order of magnitude, one water depth[2] 1). A corollary is that a drifting VLA could be used with this technique to survey the seabed.

It is possible to see similar effects at any frequency. Figure 27 shows plots for 1400 Hz.

---

[2] One could argue that the true area is an annulus of radius $z_a \cot\theta$, where z_a is array height above the seabed. Without stretching the ray or wave theory too far (with a finite length array) we can see that the relevant area has radius of order the water depth.
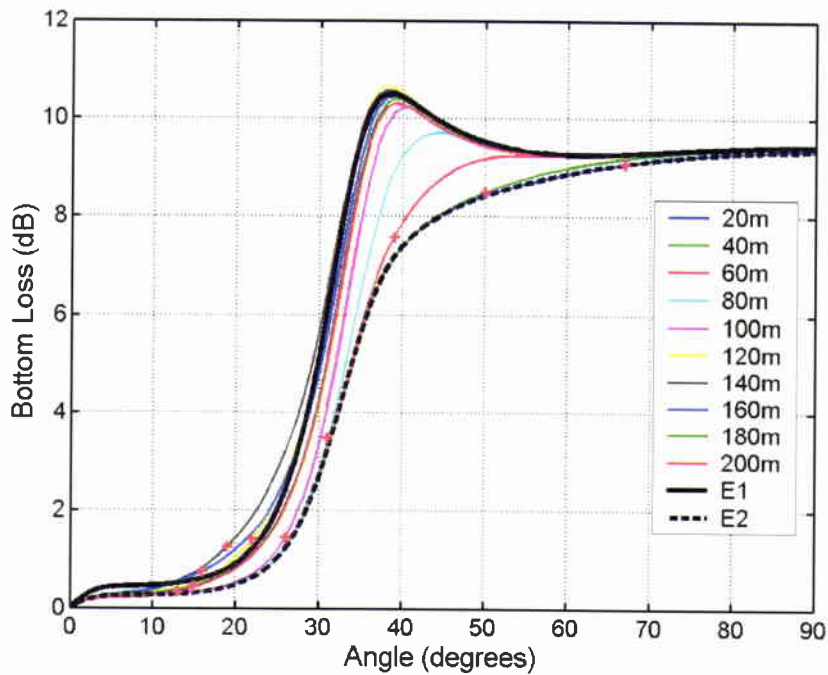
Figure 27 *Deduced bottom loss at 1400 Hz (colour-coded lines) for various sizes of bottom disk with E1 properties (three-layer, giving resonance peaks), outside which there is E2 properties (two-layer, standard Rayleigh). Red crosses indicate the angle for each coloured line at which we expect a rough transition from E2 to E1 (black lines).*

Again if we inspect each line in turn we find that for angles greater than that of the cross (angles nearer the vertical) the curve tends to the E1 thick line. Conversely for shallower angles the curve tends to the E2 thick line. Of course, at higher frequencies we expect beam side-lobe effects and edge-diffraction effects near the transition, and this is the cause of the anomalous blue and grey kinks at about 23°. Note that although we expect the solution to converge on E1 or E2 at the two extremes, the two thick lines should not be regarded as bounds between which the coloured lines should remain.

6.3 Downward refraction

Figures 28 and 29 show equivalent plots for a downward refracting environment (linear SSP with 1522m/s at the surface, 1512m/s at the seabed and 1517m/s at the centre of the array). The plot in Fig. 29 is against angle at the seabed rather than at the array. The disk radii are not identical with those in Fig. 26, but comments and conclusions are the same.

Figure 28 *Deduced bottom loss at 600 Hz (colour-coded lines) for various sizes of bottom disk with E1 properties (three-layer, giving resonance peak), outside which there is E2 properties (two-layer, standard Rayleigh). Red crosses indicate the angle for each coloured line at which we expect a rough transition from E2 to E1 (black lines). Water column is downward refracting.*
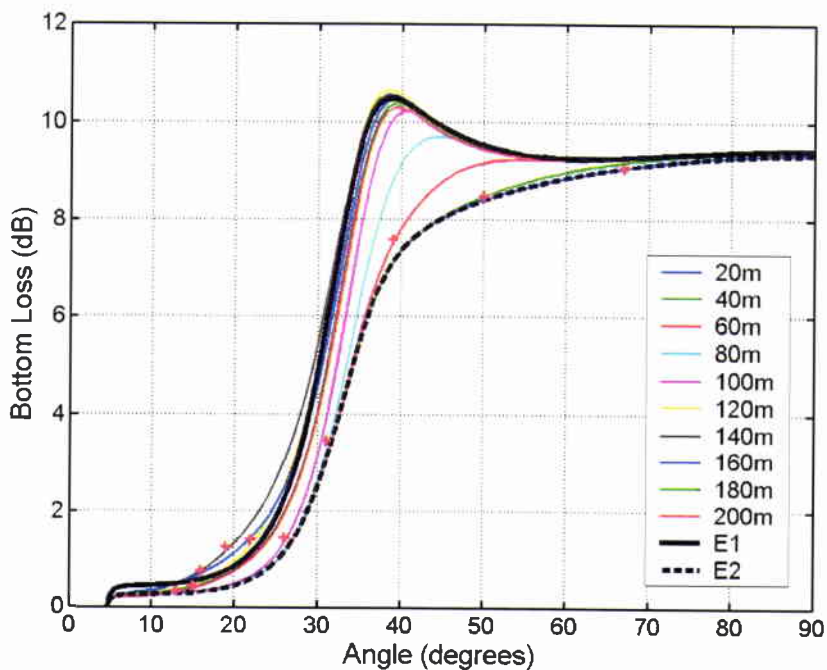
Figure 29 *Deduced bottom loss at 600 Hz (colour-coded lines) for various sizes of bottom disk with E1 properties (three-layer, giving resonance peak), outside which there is E2 properties (two-layer, standard Rayleigh). Red crosses indicate the angle for each coloured line at which we expect a rough transition from E2 to E1 (black lines). Water column is downward refracting. Angles are corrected to those at the seabed.*

7
Conclusions

A new method for deducing bottom properties from ambient noise directionality has already been proposed [1]. This report investigates possible limitations of the method, in the most part, by using numerical simulation. A number of studies have been carried out on the topics mentioned in Section 1, namely: addition of uncorrelated noise, nearby and distant point sources, absorption and refraction in the water column, array tilt, finite array length. Under the conditions that there is a reasonable wind to ship intensity ratio, none of these appear to cause any serious problems with the technique. Still the main problem is that distant shipping may provide a very strong near horizontal noise contribution which (though not important *per se*) can contaminate the steered beams through their side-lobes if winds are weak. The exact transition point has not been investigated numerically because the threshold is easy to see experimentally with a variable wind. An interesting point is whether the deduced reflection loss is a local or a spatially averaged quantity. Numerical investigations suggest that it is, in fact, local and that the technique can be used for surveying the seabed with a drifting vertical array.

– 28 –

Acknowledgement

SACLANTCEN SM-392

References

[1] Harrison, C.H., Simons, D.G. Geoacoustic inversion of ambient noise: a simple method. *Journal of the Acoustical Society of America*, 2002.

[2] Harrison, C.H., Simons, D.G. Geoacoustic inversion of ambient noise: a simple method, SACLANTCEN SM-387. La Spezia, Italy, NATO SACLANT Undersea Research Centre, 2002.

[3] Harrison, C.H., Simons, D.G. Geoacoustic inversion of ambient noise: a simple method. *Proceedings of the Institute of Acoustics*, **23**, 2001:91-98.

[4] Harrison, C.H. Bottom reflection properties by inversion of ambient noise, Proceedings of the European Conference on Underwater Acoustics, Gdansk, Poland, June 2002: pp. 471-476.

[5] Schmidt, H OASES user's guide and reference manual, Department of Ocean Engineering, M.I.T., 1999.

[6] Harrison, C.H. Formulas for ambient noise level and coherence. *Journal of the Acoustical Society of America*, **99**, 1996:2055-2066.

[7] Schmidt, H MIT private communication.

[8] Skretting, A , Leroy, C.C. Sound attenuation between 200 Hz and 10 kHz. *Journal of the Acoustical Society of America*, **49**, 1970:276-282.

[9] Breeding, J.E., Pflug, L.A., Bradley, M., Hebert, M., Wooten, M. RANDI 3.1 User's Guide. Naval Research Laboratory Report No. NRL/MR/7176—94-7552, 1994.

[10] Ferla, M.C., Porter, M.B., Jensen, F.B. C-SNAP: coupled SACLANTCEN normal mode propagation loss model, SACLANTCEN SM-274. La Spezia, Italy, NATO SACLANT Undersea Research Centre, 1993.

[11] Collins, M.D. User's guide for RAM versions 1.0 and 1.0p, NRL Report, 1996.

Document Data Sheet

Security Classification	Project No.
UNCLASSIFIED	04C-3

Document Serial No.	Date of Issue	Total Pages
SM-392	October 2002	35 pp.

Author(s)

Harrison, C.H., Baldacci, A.

Title

Bottom reflection properties deduced from ambient noise: simulation of a processing technique.

Abstract

A promising new method has already been proposed [SACLANTCEN SM-387] to calculate bottom reflection loss from ambient noise directionality. Although this method has been tried experimentally at more than 11 sites under various conditions, it is difficult to explore its limitations exhaustively by experiment. In these cases numerical testing is much more straightforward. For example, array tilt, array curvature, and varying sound speed along the array are relatively easy to model. Numerical techniques are useful in eliminating contending effects and homing in on the correct one. They also provide a second opinion on the theoretical background of the experimental technique, and throw light on, for instance, the feasibility of using a drifting array as a bottom surveying tool. This report attempts to quantify problems such as these.

Keywords

Reflection loss – array – beam-forming – ambient noise – simulation – modelling